AN ARTIFICIAL COMPRESSION REDUCED ORDER MODEL*

VICTOR DECARIA[†], TRAIAN ILIESCU[‡], WILLIAM LAYTON[†], MICHAEL MCLAUGHLIN[†], AND MICHAEL SCHNEIER[§]

Abstract. We propose a novel artificial compression, reduced order model (AC-ROM) for the numerical simulation of viscous incompressible fluid flows. The new AC-ROM provides approximations not only for velocity but also for pressure, which is needed to calculate forces on bodies in the flow and to connect the simulation parameters with pressure data. The new AC-ROM does not require that the velocity-pressure ROM spaces satisfy the inf-sup (Ladyzhenskaya–Babuska–Brezzi) condition, and its basis functions are constructed from data that are not required to be weakly divergence-free. We prove error estimates for the reduced basis discretization of the AC-ROM. We also investigate numerically the new AC-ROM in the simulation of a two-dimensional flow between offset cylinders.

Key words. Navier-Stokes equations, proper orthogonal decomposition, artificial compression

AMS subject classifications. 65M12, 65M15, 65M60

DOI. 10.1137/19M1246444

1. Introduction. We consider the Navier-Stokes equations (NSE) with no-slip boundary conditions:

(1.1)
$$u_t + u \cdot \nabla u + \nabla p - \nu \Delta u = f \text{ and } \nabla \cdot u = 0 \text{ in } \Omega \times (0, T],$$
$$u = 0 \text{ on } \partial\Omega \times (0, T] \text{ and } u(x, 0) = u_0(x) \text{ in } \Omega.$$

Here u is the velocity, f is the known body force, p is the pressure, and ν is the kinematic viscosity. For the past three decades, reduced order models (ROMs) have been successfully used in the numerical simulation of fluid flows modeled by the NSE (1.1) [4, 12, 18, 19, 21, 22, 35, 38, 39, 44]. The ROM construction is similar to the full finite element approximation except we seek a solution in a low-dimensional ROM space X_R using the basis $\{\varphi_i\}_{i=1}^R$. These basis functions are often assumed to be weakly divergence-free. This assumption holds true, for example, if the ROM basis functions are constructed from data from a NSE discretization with finite element velocity-pressure pairs that satisfy the inf-sup (Ladyzhenskaya–Babuska–Brezzi (LBB)) condition. In this case, the pressure drops out from the ROM, which yields approximations only for the velocity field, such as for the linearly implicit backward Euler method

$$\left(\frac{u_R^{n+1}-u_R^n}{\Delta t},\varphi\right)+b^*\left(u_R^n,u_R^{n+1},\varphi\right)+\nu\left(\nabla u_R^{n+1},\nabla\varphi\right)=\left(f^{n+1},\varphi\right)\quad\forall\varphi\in X_R,$$

https://doi.org/10.1137/19M1246444

Funding: The research of the first, third, and fourth authors was partially supported by NSF grants DMS 1522267 and 1817542 and CBET 1609120. The research of the second author was partially supported by NSF grant DMS 1821145.

^{*}Received by the editors February 25, 2019; accepted for publication (in revised form) December 6, 2019; published electronically February 6, 2020.

[†]Department of Mathematics, University of Pittsburgh, Pittsburgh, PA 15206 (vpd7@pitt.edu, wjl@pitt.edu, mem226@pitt.edu).

[‡]Department of Mathematics, Virginia Tech, Blacksburg, VA 24061-0123 (iliescu@vt.edu).

[§]Corresponding author. Department of Mathematics, University of Pittsburgh, Pittsburgh, PA 15206 (mhs64@pitt.edu).

where u_R^n denotes the ROM velocity approximation at time step n, $b^*(w, u, v) := \frac{1}{2}(w \cdot \nabla u, v) - \frac{1}{2}(w \cdot \nabla v, u) \ \forall u, v, w \in [H^1(\Omega)]^d$, and the superscript denotes the time step number.

We emphasize, however, that even when the pressure is not required in the ROM, one may still need a ROM pressure approximation. This happens, for example, in fluid-structure interaction problems, if drag and lift coefficients need to be computed or if the residual has to be calculated [7]. Another practical issue with velocity only ROMs is that internal (industrial) flows will often have reliable pressure data but little to no velocity data. A velocity only ROM will be unable to incorporate pressure data to improve accuracy, calibrate the model, or check if a control loop is functioning properly.

When a ROM pressure approximation is required, there are three main approaches that are currently used:

(I) Inf-sup/LBB condition. In the first approach, the velocity and pressure ROM approximations satisfy the inf-sup/LBB condition:

(1.3)
$$\inf_{q_M \in Q_M} \sup_{v_R \in X_R} \frac{\left(\nabla \cdot v_R, q_M\right)}{\left\|\nabla v_R\right\| \left\|q_M\right\|} \ge \beta_{is} > 0.$$

This approach has been extensively developed in the reduced basis method (RBM) community over the past decade [19, 38]. This approach yields accurate ROM approximations for both velocity and pressure and eliminates the spurious numerical instabilities in the pressure approximation that are often generated by ROMs that do not satisfy the inf-sup condition. Furthermore, rigorous error estimates are proven for the LBB conforming ROM approximations. The RBM has been successfully used in numerous scientific and engineering applications [19, 38]. However, enforcing the inf-sup condition (1.3) is significantly more challenging for ROMs than for finite elements. Indeed, in the finite element context, the approximation spaces (e.g., piecewise quadratic for the velocity and piecewise linear for the pressure, i.e., the Taylor-Hood element) are specified beforehand and the corresponding discrete inf-sup condition can be investigated a priori. In the ROM context, on the other hand, the approximation spaces are problem-dependent—they are known only after the underlying finite element simulations (or the actual physical experiments) have been carried out. Thus, in a ROM context, the inf-sup condition needs to be enforced for each problem separately. In the RBM context, this is generally achieved by enriching the ROM basis with supremizers, which need to be computed in the offline stage, either with a Galerkin [19, 38] or a Petrov-Galerkin [1, 49] formulation. In realistic fluid flow applications (e.g., the NSE at high Reynolds numbers), enforcing the inf-sup condition can be prohibitively expensive (see, e.g., sections 4.2.2 and 4.2.3 in [5], as well as [43]).

(II) Pressure Poisson equation. In the second approach to generate ROM approximation for the pressure, the available ROM velocity approximation is used to solve a pressure Poisson equation for the ROM pressure approximation

(1.4)
$$\Delta p_M = -\nabla \cdot ((u_R \cdot \nabla)u_R) \quad \text{in } \Omega,$$

which is obtained by taking the divergence of the NSE (1.1). This approach has been used in, e.g., [2, 7, 36, 43]. We note that this approach faces several significant challenges: We emphasize that the Poisson equation (1.4) is not valid anymore if the ROM basis functions are not weakly divergence-free. This is the case, for example, if the ROM basis functions are built from data from NSE discretizations with finite element

velocity-pressure pairs that do not satisfy the inf-sup/LBB condition, e.g., when the artificial compression, penalty, or projection methods are used [16]. Furthermore, the boundary conditions for (1.4) are not clear. Finally, the numerical investigation in [7] showed that even when weakly divergence-free snapshots were used, the ROMs that solve the pressure Poisson equation (1.4) were less competitive in terms of numerical accuracy and computational efficiency.

(III) Pressure stabilization. In the numerical discretization of the NSE (1.1) with standard numerical methods (e.g., finite elements), there are two main types of numerical instability: (i) the convective instability, which occurs in underresolved numerical simulations when the convection term dominates the diffusion term in the NSE, and (ii) the pressure instability, which occurs, e.g., when finite elements that violate the inf-sup condition are used. We emphasize that the two types of numerical instability are different (although they are often treated together) [26]. Indeed, the convective instability (i) is relevant even in equations that do not have a pressure term (e.g., convection-diffusion equations), whereas the pressure instability (ii) is relevant even in equations that do not have a convective term (e.g., the Stokes equations).

In this paper, we propose a novel pressure stabilized ROM that addresses the pressure instability. To construct the new ROM, we use the *artificial compression (AC)* method, which, together with related approaches (e.g., the penalty and projection methods) have found significant success in the CFD community [10, 13, 16].

In standard numerical discretizations (e.g., finite elements), the AC method replaces the incompressibility condition in the NSE with an AC condition. Thus, the AC method decouples the velocity and pressure computations, which results in significant savings in execution time and storage. Furthermore, since the velocity and pressure computations are decoupled, the AC method allows the use of finite element pairs that do not satisfy the inf-sup/LBB condition [30]. (We also note that, because the incompressibility condition is not satisfied exactly, the AC method yields velocity fields that are not weakly divergence-free.)

In this paper, we use the AC method to construct a novel *artificial compression ROM (AC-ROM)*, which is a pressure stabilization ROM. The fully discrete algorithm for the new AC-ROM can be written as

$$(1.5a) \qquad \left(\frac{u_R^{n+1} - u_R^n}{\Delta t}, \varphi\right) + b^* \left(u_R^n, u_R^{n+1}, \varphi\right) + \nu \left(\nabla u_R^{n+1}, \nabla \varphi\right) \\ - \left(p_M^{n+1}, \nabla \cdot \varphi\right) = \left(f^{n+1}, \varphi\right) \qquad \forall \varphi \in X_R, \\ (1.5b) \qquad \varepsilon \left(\frac{p_M^{n+1} - p_M^n}{\Delta t}, \psi\right) + \left(\nabla \cdot u_R^{n+1}, \psi\right) = 0 \qquad \forall \psi \in Q_M,$$

where $(\{\varphi_i\}_{i=1}^R, \{\psi_k\}_{k=1}^M)$ is the ROM basis for the ROM space (X_R, Q_M) . The new AC-ROM (1.5a)–(1.5b) has several significant advantages over the approaches (I) and (II):

- The AC-ROM does not require that the velocity-pressure ROM spaces satisfy the inf-sup/LBB condition, thus avoiding the challenges encountered in approach (I).
- The AC-ROM basis functions are constructed from data that do not have to be weakly divergence-free, such as those from NSE discretizations with the AC, penalty, or projection methods. Thus, the AC-ROM avoids the challenges faced by approach (II).

Stabilized ROMs addressing the convective instability (i) have been extensively investigated (see, e.g., [6, 47] and references therein). We emphasize, however, that

stabilized ROMs addressing the pressure instability (ii) have been much less investigated.

Stabilized ROMs addressing the convective and pressure instabilities monolithically were proposed in [6] (see also [46]): The residual was used to construct ROM stabilizations of streamline upwind Petrov–Galerkin (SUPG) and variational multiscale type for the convective instability. However, since the residual contained a ROM pressure term (although no ROM model was used for the pressure), the ROM stabilization in [6] could also be interpreted as ROM pressure stabilization.

In [7], although the convective and pressure instabilities were also treated together, in contrast to [6], different stabilization terms with different parameters were used for each source of instability: An SUPG term was used for the convective instability, and a pressure stabilization Petrov-Galerkin term was used for the pressure instability.

To our knowledge, the AC-ROM (1.5) is the first ROM stabilization model that exclusively targets the pressure instability. Furthermore, to our knowledge, the AC-ROM error estimates proven below represent the first instance when the parameter scalings for ROM pressure stabilization are determined through mathematical arguments instead of heuristics, as used in [6, 7, 46]. See also [40] for recent work on a related but different approach.

Additionally, we present a novel analysis for the AC-ROM (1.5). In the finite element setting it is known that AC and projection methods utilizing basis functions that do not satisfy the inf-sup condition have a decreased rate of convergence (see [16]). The novelty of our analysis is that we show in the ROM setting that this convergence rate degradation may be alleviated, based on an a priori computable value, determined by the ROM velocity and pressure spaces (see Remark 5.10). This same approach can be used for other pressure stabilized ROMs such as projection methods.

The rest of the paper is organized as follows: In section 2, we introduce some notation. In section 3, we describe the proper orthogonal decomposition, which we use to construct the ROM basis. In sections 4 and 5, we prove the stability and an error estimate of the AC-ROM (1.5a)–(1.5b), respectively. In section 6, we investigate numerically the new AC-ROM in the simulation of a two-dimensional flow between offset cylinders. Finally, in section 7, we draw conclusions and outline future research directions.

2. Notation and preliminaries. We denote by $\|\cdot\|$ and (\cdot,\cdot) the $L^2(\Omega)$ norm and inner product, respectively, and by $\|\cdot\|_{L^p}$ and $\|\cdot\|_{W^k_p}$ the $L^p(\Omega)$ and Sobolev $W^k_p(\Omega)$ norms, respectively. $H^k(\Omega) = W^k_p(\Omega)$ with norm $\|\cdot\|_k$. For a function v(x,t) that is well defined on $\Omega \times [0,T]$, we define the continuous norms

$$||v||_{L^2(a,b;L^2(\Omega))} := \left(\int_a^b ||v(\cdot,t)||^2 dt \right)^{\frac{1}{2}} \quad \text{and} \quad ||v||_{\infty} := \operatorname{ess\,sup}_{[0,T]} ||v(\cdot,t)||.$$

The space $H^{-1}(\Omega)$ denotes the dual space of bounded linear functionals defined on $H_0^1(\Omega) = \{v \in H^1(\Omega) : v = 0 \text{ on } \partial\Omega\}$; this space is equipped with the norm

$$||f||_{-1} = \sup_{0 \neq v \in X} \frac{(f, v)}{||\nabla v||} \quad \forall f \in H^{-1}(\Omega).$$

The solutions spaces X for the velocity and Q for the pressure are, respectively, defined as

$$X := [H_0^1(\Omega)]^d = \{ v \in [L^2(\Omega)]^d : \nabla v \in [L^2(\Omega)]^{d \times d} \text{ and } v = 0 \text{ on } \partial \Omega \},$$

$$Q := L_0^2(\Omega) = \left\{ q \in L^2(\Omega) : \int_{\Omega} q dx = 0 \right\}.$$

A weak formulation of the NSE is given as follows: find $u:(0,T]\to X$ and $p:(0,T]\to Q$ that, for almost all $t\in(0,T]$, satisfy

(2.1)
$$\begin{cases} (u_t, v) + (u \cdot \nabla u, v) + \nu(\nabla u, \nabla v) - (p, \nabla \cdot v) = (f, v) & \forall v \in X, \\ (\nabla \cdot u, q) = 0 & \forall q \in Q, \\ u(x, 0) = u^0(x). \end{cases}$$

We denote conforming velocity and pressure finite element spaces based on a regular triangulation of Ω having maximum triangle diameter h by $X_h \subset X$ and $Q_h \subset Q$. We also assume that the finite element spaces satisfy the approximation properties

$$\inf_{\substack{v_h \in X_h \\ v_h \in X_h}} \|v - v_h\| \le C(v)h^{s+1} \quad \forall v \in [H^{s+1}(\Omega)]^d,$$

$$\inf_{\substack{v_h \in X_h \\ q_h \in Q_h}} \|\nabla(v - v_h)\| \le C(v)h^s \quad \forall v \in [H^{s+1}(\Omega)]^d,$$

$$\inf_{\substack{q_h \in Q_h \\ q_h \in Q_h}} \|q - q_h\| \le C(q)h^k \quad \forall q \in H^k(\Omega),$$

where C is a positive constant that is independent of h.

We define the trilinear form

$$b(w, u, v) = (w \cdot \nabla u, v) \qquad \forall u, v, w \in [H^1(\Omega)]^d$$

and the explicitly skew-symmetric trilinear form given by

$$b^*(w,u,v) := \frac{1}{2}(w \cdot \nabla u, v) - \frac{1}{2}(w \cdot \nabla v, u) \qquad \forall u, v, w \in [H^1(\Omega)]^d,$$

which satisfies the bounds [30]

$$(2.2) b^*(w, u, v) \le C_{b^*}(\|w\|\|\nabla w\|)^{1/2}\|\nabla u\|\|\nabla v\| \forall u, v, w \in X,$$

$$(2.3) b^*(w, u, v) \le C_{b^*} \|\nabla w\| (\|u\| \|\nabla u\|)^{1/2} \|\nabla v\| \forall u, v, w \in X.$$

To ensure the uniqueness of the NSE solution and ensure that standard finite element error estimates hold, we make the following regularity assumptions on the data and true solution [30].

Assumption 2.1. In (2.1) we assume that $u^0 \in X$, $f \in L^2(0,T;L^2(\Omega))$, $u \in L^{\infty}(0,T;L^2(\Omega)) \cap L^4(0,T;H^{s+1}(\Omega)) \cap H^1(0,T;H^{s+1}(\Omega)) \cap H^2(0,T;L^2(\Omega))$, and $p \in L^{\infty}(0,T;Q\cap H^k(\Omega))$.

Taking N to be a positive integer, we consider a uniform discretization of the interval $[0,T], 0=t_0 < t_1 < \cdots < t_N = T$. The full space and time model on which we base our method is a backward Euler based AC scheme with a Taylor–Hood spatial discretization, i.e., P^s-P^{s-1} with $s\geq 2$. Given $u_h^0\in X_h,\ p_h^0\in Q_h$ for $n=0,1,2,\ldots,N-1$, find $u_h^{n+1}\in X_h$ and $p_h^{n+1}\in Q_h$ satisfying

$$\left(\frac{u_h^{n+1} - u_h^n}{\Delta t}, v_h\right) + b^* \left(u_h^n, u_h^{n+1}, v_h\right) + \nu \left(\nabla u_h^{n+1}, \nabla v_h\right)
- \left(p_h^{n+1}, \nabla \cdot v_h\right) = (f^{n+1}, v_h) \quad \forall v_h \in X_h,
\varepsilon \left(\frac{p_h^{n+1} - p_h^n}{\Delta t}, q_h\right) + \left(\nabla \cdot u_h^{n+1}, q_h\right) = 0 \quad \forall q_h \in Q_h.$$

We then assume the following error estimate for the finite element solution of (2.4) used to compute the velocity and pressure snapshots.

Assumption 2.2. We assume that the finite element errors satisfy the following error estimates:

$$\|u^N - u_h^N\|^2 + \|p^N - p_h^N\|^2 + \nu \Delta t \sum_{n=1}^N \|\nabla(u^n - u_h^n)\|^2 \le C(\nu, u, p) \left(h^{2s} + h^{2k} + \Delta t^2\right).$$

Remark 2.3. Error estimates of this form have been proven for (2.4) in [37]. We have implicitly assumed, as is the standard approach, that $\varepsilon = \mathcal{O}(\Delta t)$; therefore, the constant appearing on the right-hand side is independent of ε . We note that it is also possible to generate the snapshots using other stabilized schemes such as the incremental pressure correction scheme in [15]. However, depending upon the scheme used, a different assumption on the finite element error may be needed. We also note that the constant $C(\nu, u, p)$ contains the term $\exp(\frac{CT}{\nu^3})$ due to the need to use Gronwall's inequality in the finite element error analysis [30].

Lastly, we define the discrete norms

$$||v||_{2,s} := \left(\sum_{n=0}^N ||v^n||_s^2 \Delta t\right)^{\frac{1}{2}}$$
 and $||v||_{\infty,s} := \max_{0 \le n \le N} ||v^n||_s.$

3. Proper orthogonal decomposition (POD). In this section we briefly describe the POD method and apply it to the AC algorithm (2.4). A more detailed description of this method can be found in [29].

Given a positive integer N, let $0 = t_0 < t_1 < \cdots < t_N = T$ denote a uniform partition of the time interval [0,T]. Denote by $u_{h,S}^n(x) \in X_h$, $p_{h,S}^n(x) \in Q_h$, $n = 0,\ldots,N$, the finite element solution to (2.4) evaluated at $t = t_n$, $n = 1,\ldots,N$.

We denote by u_S^n and p_S^n the vector of coefficients corresponding to the finite element functions $u_{h,S}^n$ and $p_{h,S}^n$. We then define the velocity snapshot matrix \mathbb{A} and pressure snapshot matrix \mathbb{B} as

$$\mathbb{A} = \left(u_S^1, u_S^2, \dots, u_S^{N_V}\right) \ \text{ and } \ \mathbb{B} = \left(p_S^1, p_S^2, \dots, p_S^{N_P}\right),$$

i.e., the columns of $\mathbb A$ and $\mathbb B$ are the finite element coefficient vectors corresponding to the discrete snapshots. The POD method then seeks a low-dimensional basis

$$X_R := \operatorname{span}\{\varphi_i\}_{i=1}^R \subset X_h \text{ and } Q_M := \operatorname{span}\{\psi_i\}_{i=1}^M \subset Q_h,$$

which can approximate the snapshot data. Let δ_{ij} denote the Kronecker delta. These bases can be determined by solving the constrained minimization problems

(3.1)
$$\frac{1}{N+1} \min \sum_{n=0}^{N} \left\| u_{h,s}^{n} - \sum_{j=1}^{R} (u_{h,s}^{n}, \varphi_{j}) \varphi_{j} \right\|^{2}$$
 subject to $(\varphi_{i}, \varphi_{j}) = \delta_{ij}$ for $i, j = 1, \dots, R$

and

(3.2)
$$\frac{1}{N+1} \min \sum_{n=0}^{N} \left\| p_{h,s}^{n} - \sum_{j=1}^{M} (p_{h,s}^{n}, \psi_{j}) \psi_{j} \right\|^{2}$$
 subject to $(\psi_{i}, \psi_{j}) = \delta_{ij}$ for $i, j = 1, \dots, M$.

To find the solutions to (3.1)–(3.2), we use the method of snapshots [42]. Defining the correlation matrices $\mathbb{C} = \frac{1}{N+1} \mathbb{A}^T \mathbb{M} \mathbb{A}$ and $\mathbb{D} = \frac{1}{N+1} \mathbb{B}^T \mathbb{M} \mathbb{B}$, where \mathbb{M} denotes the finite element mass matrix, these problems can then be solved by considering the eigenvalue problems

$$\mathbb{C}\vec{a}_i = \lambda_i \vec{a}_i$$

and

$$\mathbb{D}\vec{b}_i = \sigma_i \vec{b}_i.$$

It can then be shown that the POD basis functions will be given by

$$\vec{\varphi}_i = \frac{1}{\sqrt{\lambda_i}} \mathbb{A} \vec{a}_i, \quad i = 1, \dots, R,$$

and

$$\vec{\psi}_i = \frac{1}{\sqrt{\sigma_i}} \mathbb{B} \vec{b}_i, \quad i = 1, \dots, M.$$

Using this POD basis we can now construct the AC-ROM algorithm. The construction is similar to the full finite element approximation except that we seek a solution in the POD space (X_R, Q_M) using the basis $(\{\varphi_i\}_{i=1}^R, \{\psi_k\}_{k=1}^M)$. The fully discrete algorithm for the AC-ROM algorithm can be written as

(3.3a)
$$\left(\frac{u_R^{n+1} - u_R^n}{\Delta t}, \varphi\right) + b^* \left(u_R^n, u_R^{n+1}, \varphi\right) + \nu \left(\nabla u_R^{n+1}, \nabla \varphi\right) - \left(p_M^{n+1}, \nabla \cdot \varphi\right) = \left(f^{j,n+1}, \varphi\right) \qquad \forall \varphi \in X_R,$$
(3.3b)
$$\varepsilon \left(\frac{p_M^{n+1} - p_M^n}{\Delta t}, \psi\right) + \left(\nabla \cdot u_R^{n+1}, \psi\right) = 0 \qquad \forall \psi \in Q_M.$$

4. Stability. In this section we prove the unconditional, nonlinear, longtime stability of the AC-ROM algorithm.

Theorem 4.1 (unconditional stability of AC-ROM). For any n, we have the energy equality

$$\|u_R^{N+1}\|^2 + \epsilon \|p_M^{N+1}\|^2 + \sum_{n=0}^N \left(\|u_R^{n+1} - u_R^n\|^2 + \epsilon \Delta t \|p_M^{n+1} - p_M^n\|^2 \right)$$
$$+ 2\Delta t \nu \sum_{n=0}^N \|\nabla u_R^{n+1}\|^2 = \|u_R^0\|^2 + \epsilon \|p_M^0\| + 2\Delta t \sum_{n=0}^N (f^{n+1}, u_R^{n+1})$$

and, letting

$$C_{stab} := \|u_R^0\|^2 + \epsilon \|p_M^0\| + \frac{4\Delta t}{\nu} \sum_{n=0}^{N} \|f^{n+1}\|_{-1}^2,$$

the energy inequality

$$\|u_R^{N+1}\|^2 + \epsilon \|p_M^{N+1}\|^2 + \sum_{n=0}^N \left(\|u_R^{n+1} - u_R^n\|^2 + \epsilon \|p_M^{n+1} - p_M^n\|^2 \right)$$
$$+ \Delta t \nu \sum_{n=0}^N \|\nabla u_R^{n+1}\|^2 \le C_{stab}.$$

Proof. Let $\varphi=2\Delta t u_R^{n+1}$ and $\psi=2\Delta t p_M^{n+1}$ in (3.3). By the polarization identity¹ and skew-symmetry of the nonlinearity, we have

$$\begin{aligned} \left\| u_R^{n+1} \right\|^2 - \left\| u_R^n \right\|^2 + \left\| u_R^{n+1} - u_R^n \right\|^2 + 2\Delta t \nu \left\| \nabla u_R^{n+1} \right\|^2 \\ - 2\Delta t (p_M^{n+1}, \nabla \cdot u_R^{n+1}) &= 2\Delta t (f^{n+1}, u_R^{n+1}), \\ \epsilon \left(\left\| p_M^{n+1} \right\|^2 - \left\| p_M^n \right\|^2 + \left\| p_M^{n+1} - p_M^n \right\|^2 \right) + 2\Delta t (\nabla \cdot u_R^{n+1}, p_M^{n+1}) &= 0. \end{aligned}$$

Adding the two equations gives

$$\begin{aligned} \left\| u_R^{n+1} \right\|^2 - \left\| u_R^n \right\|^2 + \left\| u_R^{n+1} - u_R^n \right\|^2 + \epsilon \left(\left\| p_M^{n+1} \right\|^2 - \left\| p_M^n \right\|^2 + \left\| p_M^{n+1} - p_M^n \right\|^2 \right) \\ + 2\Delta t \nu \left\| \nabla u_R^{n+1} \right\|^2 = 2\Delta t (f^{n+1}, u_R^{n+1}). \end{aligned}$$

Summing from n = 0 to N gives the energy equality above. By definition of the dual norm and Young's inequality, we have the energy inequality

$$\begin{aligned} \left\| u_{R}^{N+1} \right\|^{2} + \epsilon \left\| p_{M}^{N+1} \right\|^{2} + \sum_{n=0}^{N} \left(\left\| u_{R}^{n+1} - u_{R}^{n} \right\|^{2} + \epsilon \Delta t \left\| p_{M}^{n+1} - p_{M}^{n} \right\|^{2} \right) \\ + \Delta t \nu \sum_{n=0}^{N} \left\| \nabla u_{R}^{n+1} \right\|^{2} \leq \left\| u_{R}^{0} \right\|^{2} + \epsilon \left\| p_{M}^{0} \right\| + \frac{4\Delta t}{\nu} \sum_{n=0}^{N} \left\| f^{n+1} \right\|_{-1}^{2}, \end{aligned}$$

proving unconditional stability.

5. Error analysis. Next we provide an error analysis for the AC-ROM scheme. We begin by stating preliminary results.

Let $\mathbb{S}_R = (\nabla \varphi_i, \nabla \varphi_j)_{L^2}$ be the POD stiffness matrix, and let $||| \cdot |||_2$ denote the matrix 2-norm. It was shown in Lemma 2 in [29] that this POD basis satisfies the following inverse inequality.

Lemma 5.1 (POD inverse estimate).

(5.1)
$$\|\nabla \varphi\| \le \||S_R||_2^{1/2} \|\varphi\| \quad \forall \varphi \in X_R.$$

The norm $|||\mathbb{S}_R|||_2$ on the right-hand side of (5.1) depends on the choice of the POD basis with no universal pattern of growth with R (their number). Since R is small, $|||\mathbb{S}_R|||_2$ can be precomputed giving a precise number for the right-hand side of (5.1).

We define the L^2 projection into the velocity space X_R and the pressure space Q_M as follows.

DEFINITION 5.2. Let $P_R: L^2(\Omega) \to X_R$ and $\chi_M: L^2(\Omega) \to Q_M$ such that

(5.2)
$$(u - P_R u, \varphi) = 0 \qquad \forall \varphi \in X_R \text{ and }$$
$$(p - \chi_M p, \psi) = 0 \qquad \forall \psi \in Q_M.$$

The following lemmas provide bounds for the error between the snapshots and their projections onto the POD space. Lemma 5.3 is Proposition 1 in [29], and Lemma 5.4 is Theorem 5.3 in [41] (see also Lemma 3.2 in [24]).

 $^{{}^{1}(}a-b,a) = \frac{1}{2} ||a||^{2} - \frac{1}{2} ||b||^{2} + \frac{1}{2} ||a-b||^{2}.$

LEMMA 5.3 (L^2 POD projection error). With λ_i the eigenvalues of $\mathbb{C} = \mathbb{A}^T \mathbb{M} \mathbb{A}$, we have

(5.3)
$$\frac{1}{N+1} \sum_{n=0}^{N} \left\| u_{h,s}^{n} - \sum_{i=1}^{R} (u_{h,s}^{n}, \varphi_{i}) \varphi_{i} \right\|^{2} = \sum_{i=R+1}^{N_{V}} \lambda_{i} \quad and$$

$$\frac{1}{N+1} \sum_{n=0}^{N} \left\| p_{h,s}^{n} - \sum_{i=1}^{M} (p_{h,s}^{n}, \psi_{i}) \psi_{i} \right\|^{2} = \sum_{i=M+1}^{N_{P}} \sigma_{i}.$$

LEMMA 5.4 (H^1 POD projection error). We have

(5.4)
$$\frac{1}{N+1} \sum_{n=0}^{N} \left\| \nabla \left(u_{h,s}^{n} - \sum_{i=1}^{R} (u_{h,s}^{n}, \varphi_{i}) \varphi_{i} \right) \right\|^{2} = \sum_{i=R+1}^{N_{V}} \| \nabla \varphi_{i} \|^{2} \lambda_{i}.$$

The following error estimates then follow easily for the L^2 projection error into the velocity space X_R using Assumption 2.2 and the techniques in Lemma 3.3 in [24]. We also note that, just as in Theorem 5.11, the constants $C(\nu, u, p)$ will be large since they will contain terms of the form $\exp(CT/\nu^3)$, which are generally present in standard error estimates for the finite element discretization of the NSE [31].

Lemma 5.5. For any $u^n \in X$ the L^2 projection error into X_R satisfies the following estimates:

$$(5.5) \quad \frac{1}{N+1} \sum_{n=0}^{N} \|u^n - P_R u^n\|^2 \le C(\nu, u, p) \left(h^{2s} + h^{2k} + \Delta t^2 + \sum_{i=R+1}^{N_V} \lambda_i \right) \quad and$$

$$\frac{1}{N+1} \sum_{n=0}^{N} \|\nabla (u^n - P_R u^n)\|^2 \le C(\nu, u, p) \left(h^{2s} + h^{2k} + |||\mathbb{S}_R|||_2 (h^{2s} + h^{2k}) + (1 + |||\mathbb{S}_R|||_2) \Delta t^2 + \sum_{i=R+1}^{N_V} \|\nabla \varphi_i\|^2 \lambda_i \right).$$

Similarly for the L^2 projection into the pressure space the following can be proven.

LEMMA 5.6. For any $p^n \in Q$ the L^2 projection error satisfies the following estimates:

(5.6)
$$\frac{1}{N+1} \sum_{n=0}^{N} \|p^n - \chi_M p^n\|^2 \le C(\nu, u, p) \left(h^{2s} + h^{2k} + \Delta t^2 + \sum_{i=M+1}^{N_P} \sigma_i \right).$$

In order to prove pointwise in time error estimates we also make the following assumption, which is similar to Assumption 3.2 in [24] and Assumption A.1 in [34] (see, e.g., Remark 3.2 in [24] for rationale).

Assumption 5.7. For any $u^n \in V$ the L^2 projection error into X_R satisfies the following estimates:

(5.7)
$$\max_{n} \|u^{n} - P_{R}u^{n}\|^{2} \leq C(\nu, u, p) \left(h^{2s} + h^{2k} + \Delta t^{2} + \sum_{i=R+1}^{N_{V}} \lambda_{i}\right) \text{ and}$$

$$\max_{n} \|\nabla(u^{n} - P_{R}u^{n})\|^{2} \leq C(\nu, u, p) \left(h^{2s} + h^{2k} + |||\mathbb{S}_{R}|||_{2}(h^{2s} + h^{2k})\right)$$

$$+ (1 + |||\mathbb{S}_{R}|||_{2})\Delta t^{2} + \sum_{i=R+1}^{N_{V}} \|\nabla\varphi_{i}\|^{2}\lambda_{i}.$$

For any $p^n \in Q$ the L^2 projection error satisfies the following estimate:

(5.8)
$$\max_{n} \|p^{n} - \chi_{M} p^{n}\|^{2} \leq C(\nu, u, p) \left(h^{2s} + h^{2k} + \Delta t^{2} + \sum_{i=M+1}^{N_{P}} \sigma_{i}\right).$$

Let e_u and e_p denote the error between the true velocity and pressure solution and their POD approximations, respectively. For the error analysis we split the error for the velocity and the pressure using the L^2 projections into the spaces X_R, Q_M :

$$(5.9) e_u^{n+1} = u^{n+1} - u_R^{n+1} = u^{n+1} - P_R(u^{n+1}) + P_R(u^{n+1}) - u_R^{n+1} = \eta^{n+1} - \xi_R^{n+1}, e_p^{n+1} = p^{n+1} - p_M^{n+1} = p^{n+1} - \chi_M(p^{n+1}) + \chi_M(p^{n+1}) - p_M^{n+1} = \kappa^{n+1} - \pi_M^{n+1}.$$

We will see in Theorem 5.11 that the convergence rate faces order reduction by a power of ε^{-1} term appearing in the error bound. This occurs due to the term $(\nabla \cdot \eta^{n+1}, \pi_M^{n+1})$ arising from the continuity equation. Due to the fact the AC-ROM scheme proposed in this paper does not require the ROM velocity-pressure spaces to satisfy the LBB_h condition, this order reduction cannot be eliminated via the usual Stokes projection.² However, we will show in Theorem 5.11 that even if the basis does not satisfy the LBB_h condition this order reduction in the convergence rate will be improved by a multiplicative constant α .

To this end, we consider the subspace

(5.10)
$$X_R^{div} := \operatorname{span}\{\nabla \cdot \varphi_i\}_{i=1}^R \subset L^2(\Omega)$$

and recall from [11] the strengthened Cauchy–Buniakowskii–Schwarz (CBS) inequality commonly used in the analysis of multilevel methods [3, 11].

LEMMA 5.8. Given a Hilbert space V and two finite-dimensional subspaces $V_1 \subset V$ and $V_2 \subset V$ with trivial intersection

$$V_1 \cap V_2 = \{0\},\$$

there exists $0 \le \alpha < 1$ such that

$$|(v_1, v_2)| \le \alpha ||v_1|| ||v_2|| \quad \forall v_1 \in V_1, v_2 \in V_2.$$

Considering X_R^{div} and Q_M , we are interested in computing the exact constant α corresponding to these spaces. This is equivalent to finding the first principal angle defined as

(5.11)
$$\theta_1 := \min_{v \neq 0, \psi \neq 0} \left\{ \arccos\left(\frac{|(v, \psi)|}{\|v\| \|\psi\|}\right) \middle| v \in X_R^{div}, \psi \in Q_M \right\}$$
 with $0 < \theta_1 \le \frac{\pi}{2}$.

 $^{^{2}}$ The H^{1} projection into the discretely divergence-free subspace.

The problem of computing angles between subspaces was introduced by Jordan in 1875 [27] and studied by Friedrichs in 1937 [14]. Recently, principal angles were used to improve the accuracy of reduced basis schemes for optimization problems in [33]. They can be calculated using either QR factorization or SVD of the orthogonal bases of the spaces in Lemma 5.8, as outlined in [48]. More efficient and stable schemes for calculating principal angles were also developed in [28]. We note that due to the relatively small size of the pressure and velocity reduced basis, the QR or SVD approach is sufficient in this setting. This procedure will be briefly outlined in section 6.

Using the strengthened CBS inequality, we get the following bound on the error term arising from the continuity equation.

LEMMA 5.9. Let $u^{n+1} = u(x, t^{n+1})$ be the exact solution of the NSE, and let $\eta^{n+1} = u^{n+1} - P_R(u^{n+1})$ denote the projection error. Defining $\alpha = \cos(\theta_1)$, where θ_1 is given in (5.11), the following bound holds:

$$\left| \left(\nabla \cdot \eta^{n+1}, \psi \right) \right| \le \alpha \| \nabla \cdot \eta^{n+1} \| \| \psi \| \qquad \forall \psi \in Q_M.$$

Proof. Since u^{n+1} is the exact solution to the NSE it follows that $\nabla \cdot u^{n+1} = 0$ and therefore $(\nabla \cdot u^{n+1}, \psi) = 0 \ \forall \psi \in Q_M$. This gives

$$\left|\left(\nabla\cdot\eta^{n+1},\psi\right)\right| = \left|\left(\nabla\cdot u^{n+1} - \nabla\cdot P_R(u^{n+1}),\psi\right)\right| = \left|\left(\nabla\cdot P_Ru^{n+1},\psi\right)\right| \ \forall \psi\in Q_M.$$

It then follows from the fact that $\nabla \cdot P_R u^{n+1} \in X_R^{div}$, Lemma 5.8, and $\nabla \cdot u^{n+1} = 0$,

$$\left| \left(\nabla \cdot P_R u^{n+1}, \psi \right) \right| \le \alpha \| \nabla \cdot P_R u^{n+1} \| \| \psi \| = \alpha \| \nabla \cdot \eta^{n+1} \| \| \psi \| \ \forall \psi \in Q_M.$$

Combining this inequality with the previous equality the result follows.

Remark 5.10. This lemma gives us a better bound on the term arising from the continuity equation. We will see in the ensuing analysis that if the α term is sufficiently small it will overcome the convergence penalty from not using an inf-sup stable basis. The calculation of the constant is based on the size of the ROM velocity and pressure basis. Therefore if R and M are $\mathcal{O}(10)$ the constant can be calculated efficiently as outlined in section 6. This is in contrast with the finite element setting where the basis can be $\mathcal{O}(10^5)$ or greater and the constant cannot be computed.

We are now ready to state an error estimate for (3.3), which will show that it converges to the true solution of the NSE up to discretization and the ROM projection error. The bound will be large due to the term $\exp\left(\frac{CT}{\nu^3}\right)$ appearing on the right-hand side. This is a standard result for the NSE due to the fact that any true solution could be unstable and therefore will diverge exponentially fast. Under a stability assumption on the true solution, such as the one made in [20], errors bounds not involving this term can be obtained. Additionally, assuming stronger regularity conditions than those in Assumption 2.1, the bound in Theorem 5.11 can be improved further; see, e.g., Theorem 7.78 of [26].

We also note that the linearly implicit method we consider is frequently used because it does not require a nonlinear iterative solver, shares the unconditional energy stability of the fully implicit method, and maintains first order accuracy. The stability and analysis for the fully implicit method mirror the analysis of the linearly implicit method presented herein. The main difference is that the linearly implicit method inherits one extra consistency error term due to the treatment of the nonlinearity (see Chapter 7 of [26].

Theorem 5.11. Consider AC-ROM (3.3) and the partition $0 = t_0 < t_1 < \cdots < t_N = T$ used in section 3. Recall α , the value dependent upon the first principal angle from Lemma 5.9, e_u and e_p , the error between the ROM approximations and the true velocity and pressure, respectively, and $\eta, \xi_R, \kappa, \pi_m$, the terms arising from splitting the error in (5.9). Let C be a constant which may depend on $f, u, p, C_{b^*}, C_{stab}$, and ν but is independent of $h, \Delta t, R, M, \lambda_i, \sigma_i$, and ϵ . Under the regularity conditions made in Assumption 2.1, with $\Delta t, \nu, \varepsilon \leq 1$, it then holds that

$$\|e_{u}^{N+1}\|^{2} + \epsilon \|e_{p}^{N+1}\|^{2} + \frac{\nu}{2} \|\nabla e_{u}\|_{2,2}^{2} \leq C \left\{ (1 + |||\mathbb{S}_{R}|||_{2})(h^{2s} + h^{2k} + \Delta t^{2}) + \sum_{i=R+1}^{N_{V}} \lambda_{i} + \sum_{i=R+1}^{N_{P}} \sigma_{i} + \sum_{i=R+1}^{N_{V}} \lambda_{i} \|\nabla \varphi_{i}\|^{2} + \exp\left(\frac{CT}{\nu^{3}}\right) \left(\|\xi_{R}^{0}\|^{2} + \epsilon \|\pi_{M}^{0}\|^{2} + \Delta t\nu \|\nabla \xi_{R}^{0}\|^{2} + \epsilon + \left(\frac{\Delta t^{1/2}}{\nu^{3/2}} + \alpha^{2}\epsilon^{-1} + \frac{1}{\nu}\right) \left((1 + |||\mathbb{S}_{R}|||_{2})(h^{2s} + h^{2k} + \Delta t^{2}) + \sum_{i=R+1}^{N_{V}} \lambda_{i} \|\nabla \varphi_{i}\|^{2} \right) + \frac{\Delta t^{2}}{\nu} + \frac{1}{\nu} \sum_{i=M+1}^{N_{P}} \sigma_{i} \right) \right\}.$$

Proof. The weak solution of the NSE satisfies

(5.12)
$$\left(\frac{u^{n+1} - u^n}{\Delta t}, \varphi\right) + b^* \left(u^{n+1}, u^{n+1}, \varphi\right) + \nu \left(\nabla u^{n+1}, \nabla \varphi\right)$$
$$- \left(p^{n+1}, \nabla \cdot \varphi\right) = \left(f^{n+1}, \varphi\right) + \tau_u \left(u^{n+1}; \varphi\right),$$

(5.13)
$$\varepsilon\left(\frac{p^{n+1}-p^n}{\Delta t},\psi\right) + \left(\nabla \cdot u^{n+1},\psi\right) = \tau_p\left(p^{n+1};\psi\right),$$

where

(5.14)
$$\tau_{u}\left(u^{n+1};\varphi\right) = \left(\frac{u^{n+1} - u^{n}}{\Delta t} - u_{t}\left(t^{n+1}\right),\varphi\right),$$

$$\tau_{p}\left(p^{n+1};\psi\right) = \left(\frac{\varepsilon}{\Delta t} \int_{t^{n}}^{t^{n+1}} p_{t}(t)dt,\psi\right).$$

Now subtracting (3.3a) from (5.12) and (3.3b) from (5.13) we have

$$(5.15) \qquad \left(\frac{\xi_R^{n+1} - \xi_R^n}{\Delta t}, \varphi\right) + \nu(\nabla \xi_R^{n+1}, \nabla \varphi) - \left(\pi_M^{n+1}, \nabla \cdot \varphi\right)$$

$$= \left(\frac{\eta^{n+1} - \eta^n}{\Delta t}, \varphi\right) + \nu\left(\nabla \eta^{n+1}, \nabla \varphi\right) - \left(\kappa^{n+1}, \nabla \cdot \varphi\right)$$

$$+ b^* \left(u^{n+1}, u^{n+1}, \varphi\right) - b^* \left(u_R^n, u_R^{n+1}, \varphi\right) - \tau_u\left(u^{n+1}; \varphi\right)$$

and

(5.16)
$$\varepsilon \left(\frac{\pi_M^{n+1} - \pi_M^n}{\Delta t}, \psi \right) + \left(\nabla \cdot \xi_R^{n+1}, \psi \right) \\ = \varepsilon \left(\frac{\kappa^{n+1} - \kappa^n}{\Delta t}, \psi \right) + \left(\nabla \cdot \eta^{n+1}, \psi \right) - \tau_p \left(p^{n+1}; \psi \right).$$

Setting $\varphi = 2\Delta t \xi_R^{n+1}$ and $\psi = 2\Delta t \pi_M^{n+1}$, we use the fact that $(\frac{\eta^{n+1} - \eta^n}{\Delta t}, \xi_R^{n+1}) = 0$ and $(\frac{\kappa^{n+1} - \kappa^n}{\Delta t}, \pi_M^{n+1}) = 0$ by the definition of the L^2 projection. Adding (5.15) to (5.16) and using the polarization identity yields

$$(5.17) \left(\|\xi_{R}^{n+1}\|^{2} + \epsilon \|\pi_{M}^{n+1}\|^{2} \right) - \left(\|\xi_{R}^{n}\|^{2} + \epsilon \|\pi_{M}^{n}\|^{2} \right) + \|\xi_{R}^{n+1} - \xi_{R}^{n}\|^{2}$$

$$+ \epsilon \|\pi_{M}^{n+1} - \pi_{M}^{n}\|^{2} + 2\Delta t\nu \|\nabla \xi_{R}^{n+1}\|^{2} = 2\Delta t\nu \left(\nabla \eta^{n+1}, \nabla \xi_{R}^{n+1} \right) - 2\Delta t \left(\kappa^{n+1}, \nabla \cdot \xi_{R}^{n+1} \right)$$

$$+ 2\Delta t \left(\nabla \cdot \eta^{n+1}, \pi_{M}^{n+1} \right) + 2\Delta tb^{*} \left(u^{n+1}, u^{n+1}, \xi_{R}^{n+1} \right) - 2\Delta tb^{*} \left(u_{R}^{n}, u_{R}^{n+1}, \xi_{R}^{n+1} \right)$$

$$- 2\Delta t\tau_{u} \left(u^{n+1}; \xi_{R}^{n+1} \right) - 2\Delta t\tau_{p} \left(p^{n+1}; \pi_{M}^{n+1} \right).$$

By Cauchy–Schwarz and Young's inequality we bound the first two terms on the right-hand side of (5.17):

(5.18)
$$2\Delta t \nu \left(\nabla \eta^{n+1}, \nabla \xi_R^{n+1}\right) \le \frac{\Delta t \nu}{\delta_1} \|\nabla \eta^{n+1}\|^2 + \delta_1 \Delta t \nu \|\nabla \xi_R^{n+1}\|^2 - 2\Delta t \left(\kappa^{n+1}, \nabla \cdot \xi_R^{n+1}\right) \le \frac{\Delta t}{\nu \delta_2} \|\kappa^{n+1}\|^2 + \delta_2 \Delta t \nu \|\nabla \xi_R^{n+1}\|^2.$$

For the third term on the right of (5.17), adding and subtracting $2\Delta t(\nabla \cdot \eta^{n+1}, \pi_M^n)$ and applying Young's inequality and Lemma 5.9 yield

$$\begin{split} & 2\Delta t \left(\nabla \cdot \eta^{n+1}, \pi_M^{n+1}\right) = 2\Delta t \left(\left(\nabla \cdot \eta^{n+1}, \pi_M^{n+1} - \pi_M^n\right) + \left(\nabla \cdot \eta^{n+1}, \pi_M^n\right)\right) \\ & \leq 2\Delta t \alpha \|\nabla \eta^{n+1}\| \|\pi_M^{n+1} - \pi_M^n\| + 2\Delta t \alpha \|\nabla \cdot \eta^{n+1}\| \|\pi_M^n\| \\ & \leq \frac{\alpha^2 \Delta t^2}{\delta_3 \epsilon} \|\nabla \eta^{n+1}\|^2 + \delta_3 \epsilon \|\pi_M^{n+1} - \pi_M^n\|^2 + \frac{\Delta t \alpha^2}{\epsilon \delta_4} \|\nabla \eta^{n+1}\|^2 + \delta_4 \epsilon \Delta t \|\pi_M^n\|^2 \\ & = \frac{\alpha^2 (\delta_4 \Delta t^2 + \delta_3 \Delta t)}{\epsilon \delta_3 \delta_4} \|\nabla \eta^{n+1}\|^2 + \delta_3 \epsilon \|\pi_M^{n+1} - \pi_M^n\|^2 + \delta_4 \epsilon \Delta t \|\pi_M^n\|^2. \end{split}$$

Next, for the nonlinear terms we add and subtract $b^*(u_R^n, u^{n+1}, \xi_R^{n+1})$ and $b^*(u^n, u^{n+1}, \xi_R^{n+1})$. This yields, by skew-symmetry,

$$\begin{split} & 2\Delta tb^* \left(u^{n+1}, u^{n+1}, \xi_R^{n+1}\right) - 2\Delta tb^* \left(u_R^n, u_R^{n+1}, \xi_R^{n+1}\right) \\ & = 2\Delta tb^* \left(u^{n+1} - u^n, u^{n+1}, \xi_R^{n+1}\right) + 2\Delta tb^* \left(u_R^n, e_u^{n+1}, \xi_R^{n+1}\right) + 2\Delta tb^* \left(e_u^n, u^{n+1}, \xi_R^{n+1}\right) \\ & = 2\Delta tb^* \left(u^{n+1} - u^n, u^{n+1}, \xi_R^{n+1}\right) - 2\Delta tb^* \left(\xi_R^n, u^{n+1}, \xi_R^{n+1}\right) + 2\Delta tb^* \left(\eta^n, u^{n+1}, \xi_R^{n+1}\right) \\ & + 2\Delta tb^* \left(u_R^n, \eta^{n+1}, \xi_R^{n+1}\right). \end{split}$$

The nonlinear terms are now bounded using the Sobolev embedding theorem, Young's inequality, (2.2), and (2.3):

$$2\Delta tb^{*}\left(u^{n+1}-u^{n},u^{n+1},\xi_{R}^{n+1}\right) \leq \frac{C\Delta t^{2}}{\delta_{5}\nu} \left\|\nabla u^{n+1}\right\|^{2} \left\|\nabla u_{t}\right\|_{L^{2}(t^{n},t^{n+1};L^{2}(\Omega))}^{2}$$

$$(5.19) \qquad +\delta_{5}\Delta t\nu \left\|\nabla \xi_{R}^{n+1}\right\|^{2},$$

$$(5.20) \qquad 2\Delta tb^{*}(u_{R}^{n},\eta^{n+1},\xi_{R}^{n+1}) \leq \frac{C\Delta t}{\delta_{6}\nu} \left\|\nabla u_{R}^{n}\right\| \left\|u_{R}^{n}\right\| \left\|\nabla \eta^{n+1}\right\|^{2} +\delta_{6}\Delta t\nu \left\|\nabla \xi_{R}^{n+1}\right\|^{2},$$

$$(5.21) \qquad 2\Delta tb^{*}(\eta^{n},u^{n+1},\xi_{R}^{n+1}) \leq \frac{C\Delta t}{\delta_{7}\nu} \left\|\nabla u^{n+1}\right\|^{2} \left\|\nabla \eta^{n}\right\|^{2} +\delta_{7}\Delta t\nu \left\|\nabla \xi_{R}^{n+1}\right\|^{2},$$

$$(5.22) -2\Delta t b^*(\xi_R^n, u^{n+1}, \xi_R^{n+1}) \le \frac{C\Delta t}{\delta_8^2 \delta_9 \nu^3} \|\nabla u^{n+1}\|^4 \|\xi_R^n\|^2 + \delta_8 \Delta t \nu \|\nabla \xi_R^{n+1}\|^2 + \delta_9 \Delta t \nu \|\nabla \xi_R^n\|^2.$$

Dealing with the consistency terms, by Taylor's theorem, the Poincaré inequality, and Young's inequality we have

(5.23)
$$-2\Delta t \tau_{u} \left(u^{n+1}; \xi_{R}^{n+1}\right) \leq 2\Delta t \left\| \frac{u^{n+1} - u^{n}}{\Delta t} - u_{t}(t^{n+1}) \right\| \|\xi_{R}^{n+1}\|$$

$$\leq \frac{C\Delta t^{2}}{\nu \delta_{10}} \|u_{tt}\|_{L^{2}(t^{n}, t^{n+1}; L^{2})}^{2} + \nu \Delta t \delta_{10} \|\nabla \xi_{R}^{n+1}\|^{2},$$

and, by adding and subtracting $2\Delta t \tau_p(p^{n+1}; \pi_M^n)$, we have

(5.24)
$$-2\Delta t \tau_{p} \left(p^{n+1}; \pi_{M}^{n+1}\right) \leq \frac{C\epsilon \Delta t}{\delta_{11}} \left\|p_{t}\right\|_{L^{2}(t^{n}, t^{n+1}; L^{2}(\Omega))}^{2} + \frac{\epsilon \Delta t}{\delta_{12}} \left\|p_{t}\right\|_{\infty}^{2} + \delta_{11}\epsilon \left\|\pi_{M}^{n+1} - \pi_{M}^{n}\right\|^{2} + \delta_{12}\epsilon \Delta t \left\|\pi_{M}^{n}\right\|^{2}.$$

Letting $\delta_1 = \delta_2 = \delta_5 = \delta_6 = \delta_7 = \delta_8 = \delta_{10} = \frac{1}{14}$, $\delta_3 = \delta_{11} = \frac{1}{4}$, $\delta_4 = \delta_{12} = \delta_9 = \frac{1}{2}$ and rearranging/combining terms we have

$$\begin{split} \left(\|\xi_{R}^{n+1}\|^{2} + \epsilon \|\pi_{M}^{n+1}\|^{2} \right) - \left(\|\xi_{R}^{n}\|^{2} + \epsilon \|\pi_{M}^{n}\|^{2} \right) + \|\xi_{R}^{n+1} - \xi_{R}^{n}\|^{2} \\ + \frac{\epsilon}{2} \|\pi_{M}^{n+1} - \pi_{M}^{n}\|^{2} + \frac{\nu \Delta t}{2} \|\nabla \xi_{R}^{n+1}\|^{2} + \frac{\nu \Delta t}{2} \left(\|\nabla \xi_{R}^{n+1}\|^{2} - \|\nabla \xi_{R}^{n}\|^{2} \right) \leq \epsilon \Delta t \|\pi_{M}^{n}\|^{2} \\ + C \Delta t \nu \|\nabla \eta^{n+1}\|^{2} + \frac{C \Delta t \alpha^{2}}{\epsilon} \|\nabla \eta^{n+1}\|^{2} + \frac{C \Delta t^{2}}{\nu} \|\nabla u^{n+1}\| \|\nabla u_{t}\|_{L^{2}(t^{n}, t^{n+1}; L^{2}(\Omega))}^{2} \\ + \frac{C \Delta t}{\nu} \|\kappa^{n+1}\|^{2} + \frac{C \Delta t^{2} \alpha^{2}}{\epsilon} \|\nabla \eta^{n+1}\|^{2} + \frac{C \Delta t}{\nu} \|u_{R}^{n}\| \|\nabla u_{R}^{n}\| \|\nabla \eta^{n+1}\|^{2} \\ + \frac{C \Delta t}{\nu} \|\nabla u^{n+1}\|^{2} \|\nabla \eta^{n}\|^{2} + \frac{C \Delta t}{\nu^{3}} \|\nabla u^{n+1}\|^{4} \|\xi_{R}^{n}\|^{2} + \frac{C \Delta t^{2}}{\nu} \|u_{tt}\|_{L^{2}(t^{n}, t^{n+1}; L^{2})}^{2} \\ + C \epsilon \Delta t \|p_{t}\|_{L^{2}(t^{n}, t^{n+1}; L^{2}(\Omega))}^{2} + C \epsilon \Delta t \|p_{t}\|_{\infty}^{2} \,. \end{split}$$

We note by Theorem 4.1 and the Cauchy-Schwarz inequality that it follows that

(5.25)

$$\begin{split} \Delta t \sum_{n=0}^{N} \|u_{R}^{n}\| \|\nabla u_{R}^{n}\| \|\nabla \eta^{n+1}\|^{2} &\leq \max_{n=0,\dots,N} \|u_{R}^{n}\| \Delta t \sum_{n=0}^{N} \|\nabla u_{R}^{n}\| \|\nabla \eta^{n+1}\|^{2} \\ &\leq \max_{n=0,\dots,N} \|u_{R}^{n}\| \left(\Delta t \sum_{n=0}^{N} \|\nabla u_{R}^{n}\|^{2}\right)^{\frac{1}{2}} \left(\Delta t \sum_{n=0}^{N} \|\nabla \eta^{n+1}\|^{4}\right)^{\frac{1}{2}} \\ &\leq \frac{C_{stab}}{\nu^{1/2}} \left(\Delta t \sum_{n=0}^{N} \|\nabla \eta^{n+1}\|^{4}\right)^{\frac{1}{2}}. \end{split}$$

By Assumption 2.1, dropping unneeded terms on the left-hand side, combining all inequalities, taking a maximum C over all constants, and summing from n=0 to N yield

$$\begin{split} \left\| \xi_{R}^{N+1} \right\|^{2} + \epsilon \left\| \pi_{M}^{N+1} \right\|^{2} + \frac{\nu}{2} \left\| \nabla \xi_{R} \right\|_{2,2}^{2} \\ & \leq \left\| \xi_{R}^{0} \right\|^{2} + \epsilon \left\| \pi_{M}^{0} \right\|^{2} + \Delta t \nu \left\| \nabla \xi_{R}^{0} \right\|^{2} + \frac{C \Delta t}{\nu^{3}} \sum_{n=0}^{N} \left(\left\| \xi_{R}^{n} \right\|^{2} + \epsilon \left\| \pi_{M}^{n} \right\|^{2} \right) \\ & + C \left[\left(\frac{1}{\nu} + (\alpha^{2} + \alpha^{2} \Delta t) \varepsilon^{-1} \right) \left\| \nabla \eta \right\|_{2,2}^{2} + \frac{1}{\nu} \left\| \kappa \right\|_{2,2}^{2} + \\ & \frac{\Delta t}{\nu} \sum_{n=0}^{N} \left\| u_{R}^{n} \right\| \left\| \nabla u_{R}^{n} \right\| \left\| \nabla \eta^{n+1} \right\|^{2} + \frac{\Delta t^{2}}{\nu} \left\| u_{tt} \right\|_{L^{2}(0,T;L^{2}(\Omega))}^{2} \\ & + \frac{\Delta t^{2}}{\nu} \left\| \nabla u_{t} \right\|_{L^{2}(0,T;L^{2}(\Omega))}^{2} + \varepsilon \Delta t \left\| p_{t} \right\|_{L^{2}(0,T;L^{2}(\Omega))}^{2} + \varepsilon \left\| p_{t} \right\|_{\infty}^{2} \right]. \end{split}$$

Therefore, by a discrete Gronwall inequality, inequality (5.25), and again taking a maximum constant we have

$$\begin{split} \left\| \xi_{R}^{N+1} \right\|^{2} + \epsilon \left\| \pi_{M}^{N+1} \right\|^{2} + \frac{\nu}{2} \left\| \nabla \xi_{R} \right\|_{2,2}^{2} \\ & \leq C \exp \left(\frac{CT}{\nu^{3}} \right) \left(\left\| \xi_{R}^{0} \right\|^{2} + \epsilon \left\| \pi_{M}^{0} \right\|^{2} + \Delta t \nu \left\| \nabla \xi_{R}^{0} \right\|^{2} \right. \\ & + \left(\frac{1}{\nu} + \alpha^{2} \varepsilon^{-1} \right) \left\| \nabla \eta \right\|_{2,2}^{2} + \frac{1}{\nu} \left\| \kappa \right\|_{2,2}^{2} + \frac{\Delta t^{2}}{\nu} \left\| u_{tt} \right\|_{L^{2}(0,T;L^{2}(\Omega))}^{2} \\ & + \left. \frac{\Delta t^{2}}{\nu} \left\| \nabla u_{t} \right\|_{L^{2}(0,T;L^{2}(\Omega))}^{2} + \frac{\Delta t^{1/2}}{\nu^{3/2}} \left(\sum_{n=0}^{N} \left\| \nabla \eta^{n+1} \right\|^{4} \right)^{\frac{1}{2}} \\ & + \varepsilon \Delta t \left\| p_{t} \right\|_{L^{2}(0,T;L^{2}(\Omega))}^{2} + \varepsilon \left\| p_{t} \right\|_{\infty}^{2} \right). \end{split}$$

By the triangle inequality we have $\|e_u^{n+1}\|^2 \le 2(\|\eta^{n+1}\|^2 + \|\xi_R^{n+1}\|^2)$, as well as $\|e_p^{n+1}\|^2 \le 2(\|\kappa^{n+1}\|^2 + \|\pi_M^{n+1}\|^2)$. Applying this and taking a maximum among constants we then have

$$\begin{split} \left\| e_{u}^{N+1} \right\|^{2} + \epsilon \left\| e_{p}^{N+1} \right\|^{2} + \frac{\nu}{2} \left\| \nabla e_{u} \right\|_{2,2}^{2} &\leq \left\| \eta^{N+1} \right\|^{2} + \epsilon \left\| \kappa^{N+1} \right\|^{2} + \frac{\nu}{2} \left\| \nabla \eta \right\|_{2,2}^{2} \\ &+ C \exp\left(\frac{CT}{\nu^{3}} \right) \left(\left\| \xi_{R}^{0} \right\|^{2} + \epsilon \left\| \pi_{M}^{0} \right\|^{2} + \Delta t \nu \left\| \nabla \xi_{R}^{0} \right\|^{2} + \left(\frac{1}{\nu} + \alpha^{2} \varepsilon^{-1} \right) \left\| \nabla \eta \right\|_{2,2}^{2} \\ &+ \frac{1}{\nu} \left\| \kappa \right\|_{2,2}^{2} + \frac{\Delta t^{2}}{\nu} \left\| u_{tt} \right\|_{L^{2}(0,T;L^{2}(\Omega))}^{2} + \frac{\Delta t^{2}}{\nu} \left\| \nabla u_{t} \right\|_{L^{2}(0,T;L^{2}(\Omega))}^{2} \\ &+ \frac{\Delta t^{1/2}}{\nu^{3/2}} \left(\sum_{n=0}^{N} \left\| \nabla \eta^{n+1} \right\|^{4} \right)^{\frac{1}{2}} + \varepsilon \Delta t \left\| p_{t} \right\|_{L^{2}(0,T;L^{2}(\Omega))}^{2} + \varepsilon \left\| p_{t} \right\|_{\infty}^{2} \right). \end{split}$$

Applying the estimates from Assumption 5.7, using the regularity from Assumption 2.1, and rearranging terms, the result follows.

Remark 5.12. We see in Theorem 5.11 whether the convergence rate is negatively impacted by ε^{-1} depends upon the constant α . The full term which arises is $\alpha^2 \varepsilon^{-1} \|\nabla \eta\|_{2,2}^2$. As the number of basis functions R grows we expect the term $\|\nabla \eta\|_{2,2}^2$ to be sufficiently small such that the term $\alpha^2 \varepsilon^{-1} \|\nabla \eta\|_{2,2}^2$ will not become the dominant error term in Theorem 5.11. Therefore we are interested in the regime where

the number of basis functions R is small and the term $\alpha^2 \varepsilon^{-1}$ dominates. In practice R will generally be taken relatively small, so this case is of particular interest. It will hold that if $\alpha^2 << \varepsilon$, then the convergence degradation caused by ε^{-1} will be alleviated.

In order for the term α^2 to be small enough to overcome the term ε^{-1} the angle between X_R^{div} and Q_M must be close to $\frac{\pi}{2}$. If the POD modes had been constructed using discretely divergence-free velocity data, then it would hold that $\alpha=0$, since the space X_R^{div} would be orthogonal to Q_M by construction. However, this is not true for the case analyzed in Theorem 5.11 where the basis is constructed using an AC scheme. In this situation it does not generally hold that α^2 is smaller than ε^{-1} . It will, however, be shown in the numerical experiments in section 6 that this may hold for small values of R.

- 6. Numerical experiments. In this section, we perform a numerical investigation of the new AC-ROM algorithm (3.3). First, we show that the AC-ROM algorithm yields accurate velocity and pressure approximations without enforcing the LBB condition or requiring weakly divergence-free snapshots. Then, we illustrate numerically the theoretical scalings proved in Theorem 5.11. In particular, we show that the AC-ROM algorithm yields first order scalings with respect to the time step, Δt . All computations are done using the FEniCS software suite [32], and all meshes generated via the built in meshing package **mshr**.
- **6.1. Problem setting.** For the numerical experiments we consider the two-dimensional flow between offset cylinders used in [17, 25]. The domain is a disk with a smaller off-center disc inside. Let $r_1 = 1$, $r_2 = 0.1$, $c_1 = 1/2$, and $c_2 = 0$; then, the domain is given by

$$\Omega = \{(x,y) : x^2 + y^2 \le r_1^2 \text{ and } (x - c_1)^2 + (y - c_2)^2 \ge r_2^2 \}.$$

The viscosity is $\nu = \frac{1}{100}$ and the body force is given by

$$f(x) = (-4y(1-x^2-y^2), 4x(1-x^2-y^2)).$$

The L^2 -POD basis is computed from snapshots of the finite element discretization of a backward Euler AC scheme.

Remark 6.1. We emphasize that since the snapshots are generated using an AC scheme they will not be weakly divergence-free. This is clearly illustrated in Figure 6.1, where we plot the divergence of the velocity basis elements, φ_i . We note that ROMs based on the pressure Poisson equation (i.e., ROMs in approach (II) in section 1) cannot be used when the snapshots are not weakly divergence-free.

For the offline calculation, the flow is initialized at rest $(u_h^0 \equiv 0 \text{ and } p_h^0 \equiv 0)$. We discretized in space via the P^2 - P^1 Taylor–Hood element pair. The spaces X_h and Q_h had 114,224 and 14,421 degrees of freedom, respectively. We took $\Delta t = 2.5e - 4$ and $\varepsilon = 1e - 6$. The mesh is shown in Figure 6.2. The no-slip, no-penetration boundary conditions are imposed on both cylinders. The flow developed into an almost periodic flow after t = 12. Velocity and pressure snapshots were taken for every $t \in [12, 16]$. The resulting singular values are shown in Figure 6.3. The POD modes corresponding to the six largest singular values for velocity (resp., pressure) are shown in Figure 6.4 (resp., Figure 6.5).

Remark 6.2. We emphasize that the new AC-ROM can use the same number of velocity and pressure basis functions, i.e., R = M in (3.3). Thus, we expect that

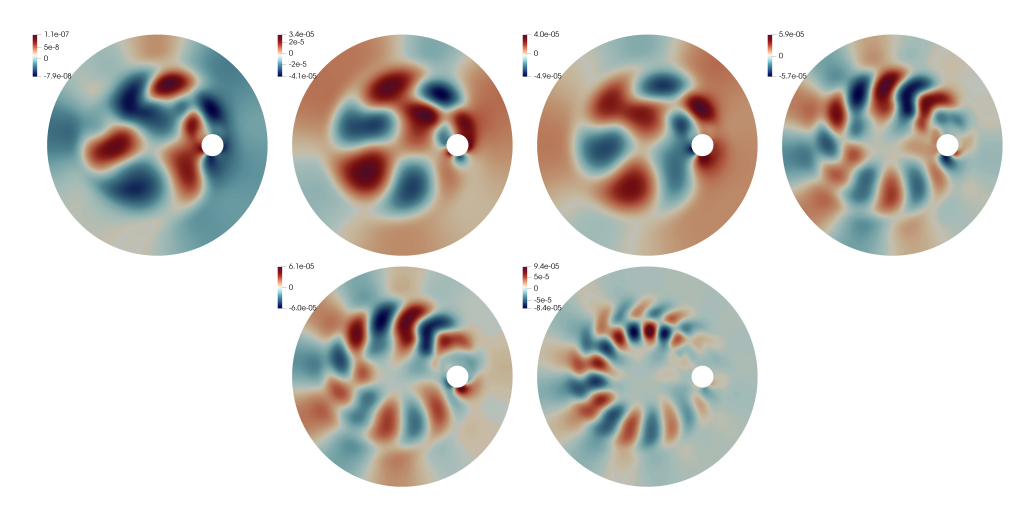
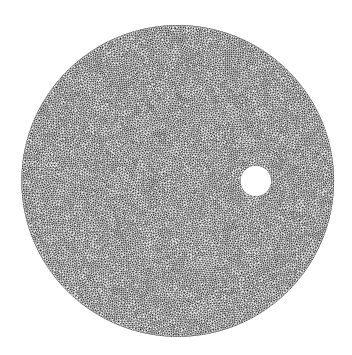
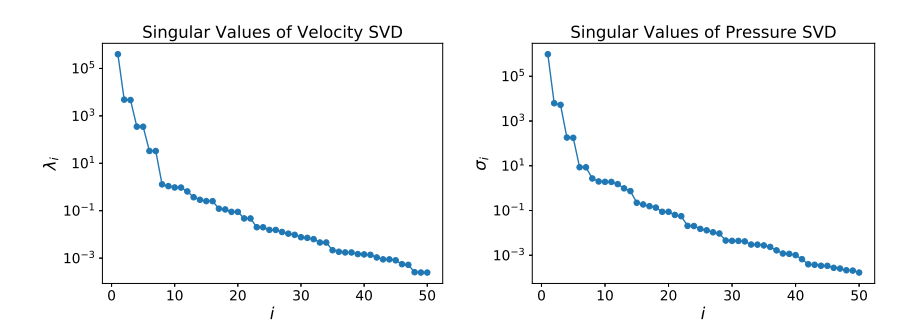


Fig. 6.1. $\nabla \cdot \varphi_i(x)$ with i from 1 (top left) to 6 (bottom right).



 ${\bf Fig.~6.2.~} {\it Spatial~mesh~for~the~finite~element~approximation}.$



 $Fig.\ 6.3.\ Singular\ values\ of\ the\ first\ 50\ modes\ for\ pressure\ and\ velocity.$

the ROM LBB condition (1.3) is not satisfied. This shows that the new AC-ROM avoids the ROM LBB condition, which is generally prohibitively expensive for the RBM methods in approach (I) of section 1 when those are used in realistic flows (see, e.g., sections 4.2.2 and 4.2.3 in [5]).

The force due to drag is the force exerted by the smaller cylinder against the main flow, which is counterclockwise. We calculated this as the line integral of the stress

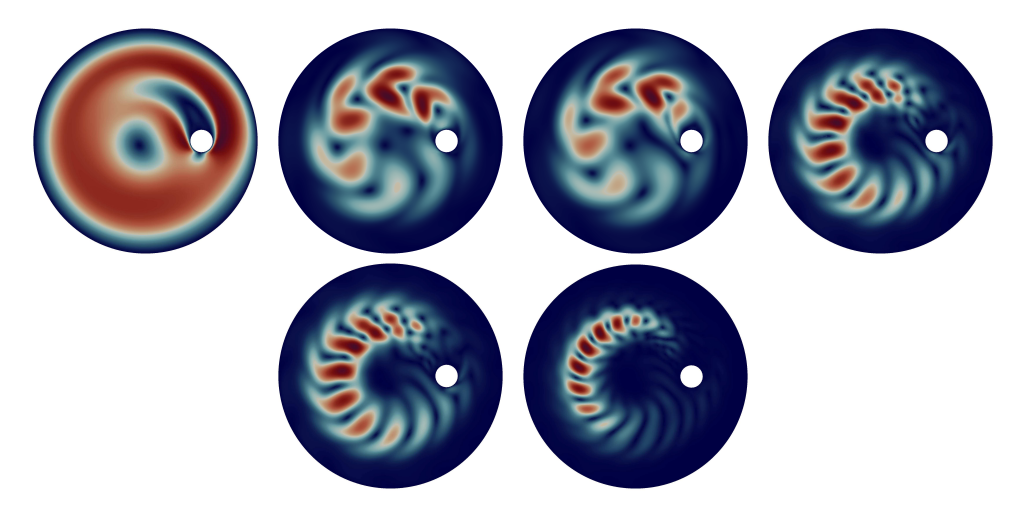


Fig. 6.4. Magnitude of velocity basis, $|\varphi_i(x)|$, with i from 1 (top left) to 6 (bottom right). Red indicates faster flow.

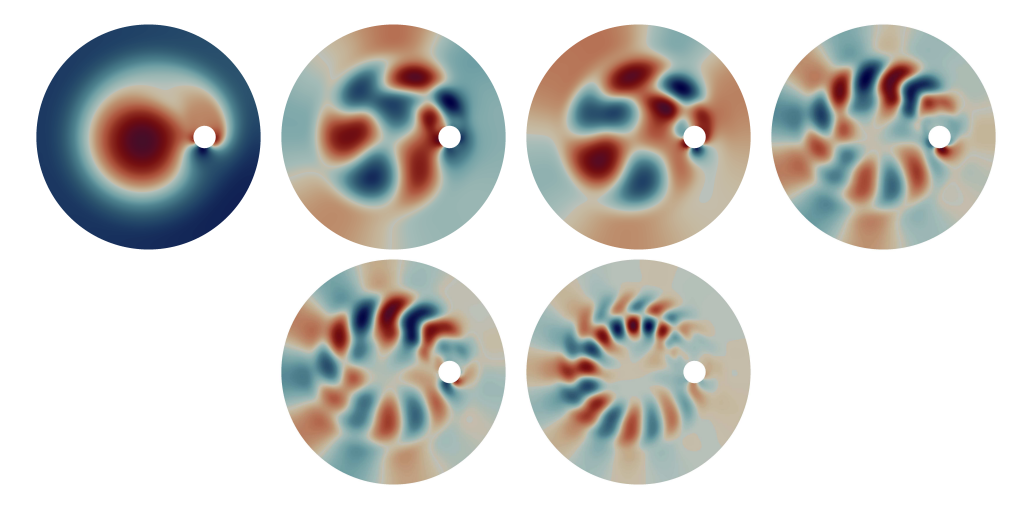


Fig. 6.5. $\psi_i(x)$ with i from 1 (top left) to 6 (bottom right).

tensor around the smaller cylinder dotted with (0, -1). The force due to lift is the line integral of the stress tensor around the smaller cylinder dotted with (1, 0).

With the stress tensor $\tau = (\nabla u + (\nabla u)^T) - pI$, and Γ_{small} the boundary restricted to the inner cylinder, these quantities are

(6.1) force due to drag =
$$-\int_{\Gamma_{small}} \tau ds \cdot e_2$$
,

$$\text{force due to lift} = \int_{\Gamma_{small}} \tau ds \cdot e_1.$$

6.2. Lift, drag, and kinetic energy. We compare the kinetic energy, force due to drag, and force due to lift of the ROM simulations with R = M = 3, 5, and 7 with the offline simulation in Figure 6.6. We construct the reduced basis from every snapshot captured on the interval $t \in [12, 16]$ and use the same Δt of 2.5×10^{-4} as in

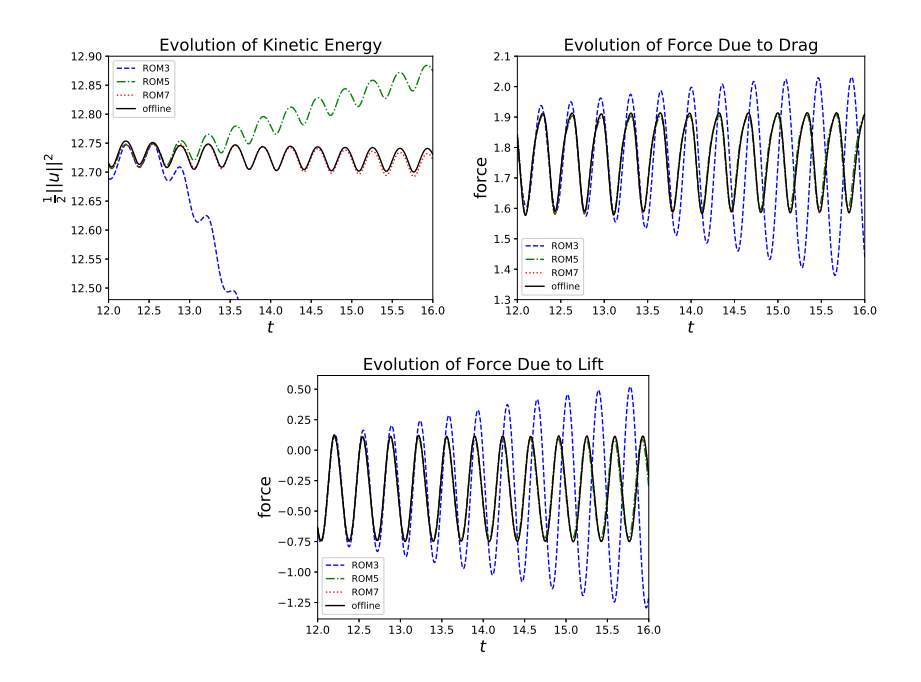


Fig. 6.6. Evolution of the energy, drag, and lift for AC-ROM with varying basis cardinality compared to the benchmark.

the offline stage. $R \ge 7$ appears sufficient to capture the kinetic energy, lift, and drag accurately. Again, this is in spite of the fact that the LBB condition is not satisfied due to using an equal number of pressure and velocity modes (see Remark 6.2).

6.3. Convergence tests. Next, to illustrate numerically the theoretical scalings proved in Theorem 5.11, we show that the new AC-ROM algorithm yields first order scalings with respect to the time step, Δt . To test convergence, we consider the error on the smaller interval $t \in [12, 12.24]$. We construct a new reduced basis from the 960 snapshots computed in this interval in the offline simulation. Then, using a fixed number of basis elements, we compute the l^2L^2 error for Δt ranging from 1.6e-2 to 2.5e-4, which was the stepsize from the offline simulation. The error is measured by comparing the u_R to the corresponding offline solution u_h . The admissible stepsizes satisfy $\Delta t_{\text{online}} = 2^i \Delta t_{\text{offline}}$ so that snapshot data exist to compute errors. The relative l^2L^2 errors that are shown in Figure 6.7 verify the $\mathcal{O}(\Delta t)$ convergence proven

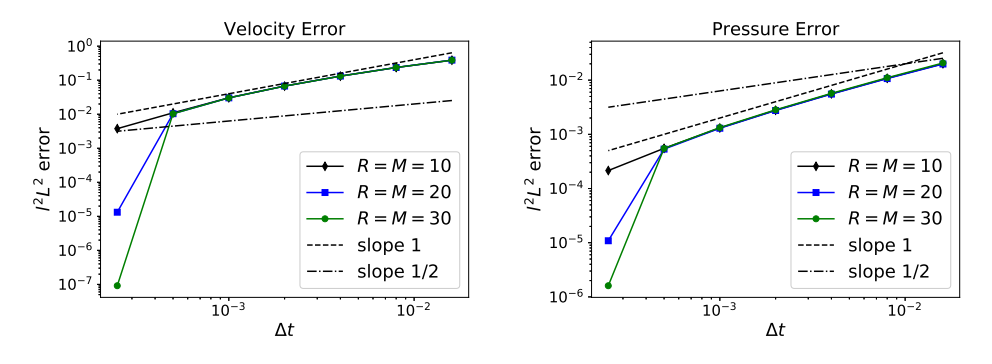


Fig. 6.7. Both the pressure and velocity are first order convergent.

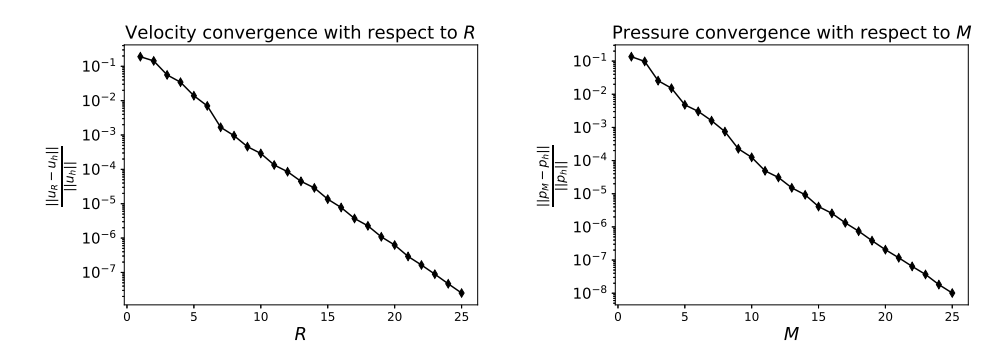


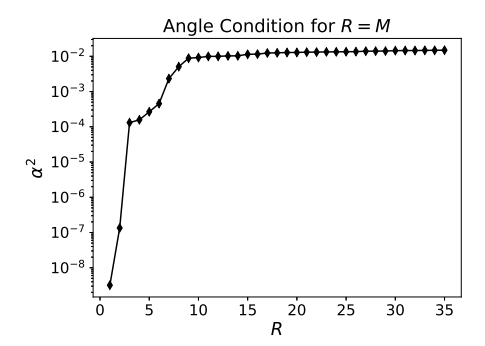
Fig. 6.8. Adding more basis functions reduces the error.

in Theorem 5.11. We also verify that error reduces when adding more basis functions. Again, for simplicity, we use an equal number of basis functions for velocity and pressure. The convergence for increasing R (and M) values is shown in Figure 6.8.

We briefly outline the process of computing the first principal angle between the spaces X_R^{div} and Q_M . Let $\{\nabla \cdot \varphi_i^{orth}\}_{i=1}^R$ denote the orthonormalized basis of X_R^{div} (5.10). We consider the matrices $\mathbb{Q} = [\psi_1, \psi_2, \dots \psi_M]$ and $\mathbb{X} = [\nabla \cdot \varphi_2^{orth}, \nabla \cdot \varphi_2^{orth}, \dots \nabla \cdot \varphi_R^{orth}]$. Multiplying these two matrices and taking the SVD gives

$$\mathbb{X}^{\top} \mathbb{Q} = U \Sigma V.$$

The first principal angle will then be given in terms of the first nonzero entry of Σ by $\theta_1 = \arccos(\sigma_1)$. We measured the influence of the principal angle between the velocity and pressure POD basis using the method outlined above. The results are shown in Figure 6.9. For small R values, α^2 begins near 10^{-8} and seems to plateau around 10^{-2} when adding more basis functions. This appears to match up with our theoretical results and explains why we do not observe an order reduction in our numerical investigation. Figure 6.10 shows the change of the inverse inequality constant, i.e., $|||\mathbb{S}|||_2^{1/2}$, with respect to the size of the velocity basis. While there is no known universal scaling law [23, 45], for this test problem, the constant appears to increase linearly with respect to R (which is precisely the scaling yielded by the Fourier basis; see equation (3.10) in Remark 3.3 in [23]) until it reaches a plateau (see Figure 5 in [23] for similar behavior).



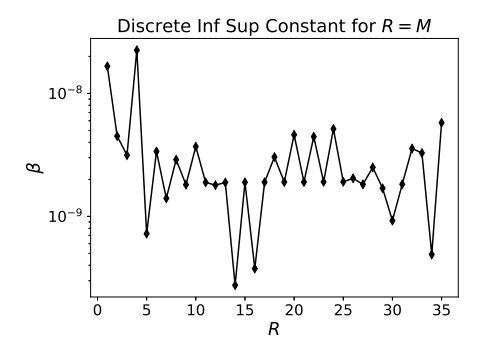


FIG. 6.9. Value of α^2 for equal number of velocity and pressure basis functions on the left and the corresponding inf-sup constant on the right.

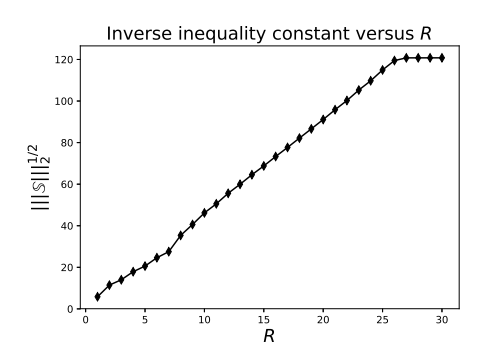


Fig. 6.10. The constant for the inverse inequality increases linearly with R until it plateaus.

- **6.4. Sensitivity analysis.** In order to verify the robustness of the method, we perform a sensitivity analysis on the online ε , which we denote by ε_{ON} . Recall that the offline solution, denoted u_h , was captured with a value of $\varepsilon = 10^{-6}$, so we are interested in determining the range of ε_{ON} that produces acceptable results. We compare the following two methods:
 - (i) The AC-ROM (3.3), for varying values of ε_{ON} against finite element based artificial compression method (AC-FEM) (2.4), with fixed $\varepsilon = 10^{-6}$.
 - (ii) The AC-ROM (3.3), for varying values of ε_{ON} against a semi-implicit backward Euler discretization of the NSE (noAC-FEM), which is given by (2.4) with $\varepsilon = 0$.

For these comparisons the same time step Δt , mesh, and Taylor–Hood finite element pair are used for each scheme. We denote the noAC-FEM solution \tilde{u}_h . We take the mean flow to be the time averaged solution over the interval [12, 16] and denote the averaging operator by $\langle \cdot \rangle$. The reduced basis from the whole interval [12, 16] is used for these tests. For each online solution u_R , we calculate two relative differences,

$$\frac{\parallel \langle u_R \rangle - \langle u_h \rangle \parallel}{\parallel \langle u_h \rangle \parallel} \qquad \text{ and } \qquad \frac{\parallel \langle u_R \rangle - \langle \tilde{u}_h \rangle \parallel}{\parallel \langle \tilde{u}_h \rangle \parallel},$$

and we try different combinations of R, M. Figure 6.11 shows the relative differences of the AC-ROM solution with different ε_{ON} against the AC-FEM solution and the noAC-FEM solution. As expected, the AC-ROM velocities are closer to the AC-FEM velocities but still agree up to two significant digits with the noAC-FEM solution for a large range of ε_{ON} .

The AC-ROM mean flow error and the divergence are insensitive for values of ε_{ON} larger than 10^{-6} , and as expected, the best AC-ROM error against the AC-FEM solution is attained for $\varepsilon_{ON}=10^{-6}$, which is the value for which the snapshots are generated. For smaller values, the AC-ROM error begins to diverge, and the divergence $\|\nabla\cdot()\|$ quickly shrinks (see Figure 6.12). This is a type of locking (see, e.g., [8]) where better mass conservation is achieved at the expense of accuracy. By penalizing divergence in the AC-ROM solution more than the AC-FEM solution, the AC-ROM solution is forced into a smaller subspace to satisfy the divergence-free constraint. For standard (e.g., finite element) discretizations, this behavior is observed for similar methods such as grad-div stabilization when the solution is penalized into a divergence-free subspace that does not have good approximation properties (see, e.g., [8]).

The AC-ROM error against the noAC-FEM mean pressure is not good, but this may be due to a poor pressure solution from the noAC-FEM formulation. Since

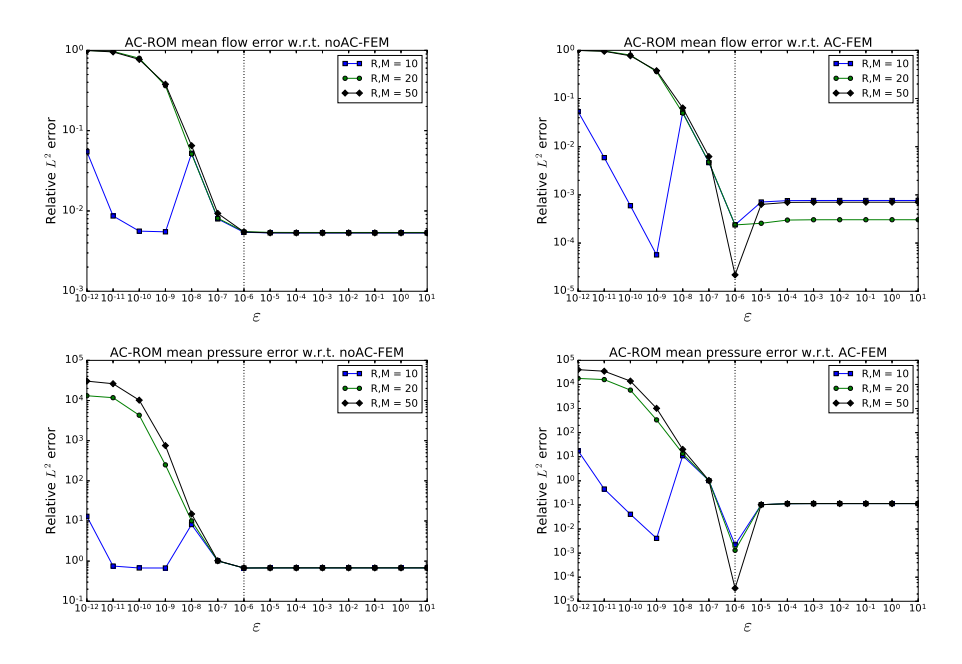


FIG. 6.11. For both the noAC-FEM and AC-FEM mean flows, the AC-ROM mean flow error is insensitive for ε_{ON} larger than the offline $\varepsilon=10^{-6}$, which is shown at the vertical dotted line. The error is minimized when the online ε_{ON} equals the offline ε and then increases for smaller values.

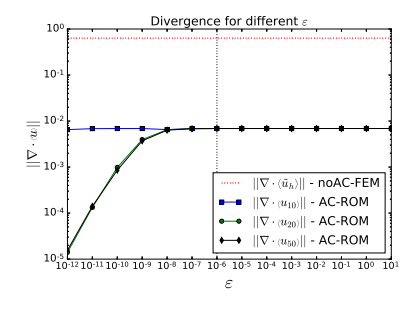


Fig. 6.12. Mean error in the divergence for varying values of ε , R, and M.

pressure enforces mass conservation, it is reasonable to expect that the large errors in $\nabla \cdot u$ in the weakly incompressible solution (displayed in Figure 6.12) will produce large errors in the pressure.

7. Conclusions and outlook. In this paper, we propose an AC-ROM for the numerical simulation of fluid flows. The new AC-ROM provides approximations for both the velocity and the pressure. Compared to the current ROMs that generate pressure approximations, the new AC-ROM has two main advantages: (i) it does not require the fulfillment of the inf-sup/LBB condition, which can be prohibitively expensive in current ROMs [7], and (ii) it does not require weakly divergence-free snapshots, which allows it to work with snapshots generated with, e.g., AC, penalty, or projection methods.

In section 4, we prove the unconditional stability of the finite element discretization of the new AC-ROM. In section 5, we prove an error estimate for the AC-ROM. In particular, we show that that it is possible to overcome the Δt^{-1} order degradation

due to lack of inf-sup stability if the angle between the divergence of the velocity space and pressure space is sufficiently small.

In section 6, we perform a numerical investigation of the new AC-ROM for a two-dimensional flow between two offset cylinders. To generate the snapshots, we use the AC method. Thus, the snapshots used in the AC-ROM construction are not weakly divergence-free, which is illustrated in Figure 6.1. We also show that the velocity and pressure spaces of the new AC-ROM do not satisfy the LBB condition (see Figure 6.9, right). In the numerical investigation of the new AC-ROM, we first show that the AC-ROM yields results that are close to the full order model results. Specifically, in Figure 6.6, we show that it provides energy, drag force, and lift force approximations that are close to the direct numerical simulation results. Next, to illustrate numerically the theoretical scalings proved in section 5, we show that the new AC-ROM algorithm yields first order scalings with respect to the time step. Finally, in Figure 6.9, we show that the constant multiplying the Δt^{-1} term in the error estimate is extremely small. This may explain why we do not observe an order reduction in our numerical investigation.

One future research direction will be a further study of the principal angle and its impact on the convergence of the AC-ROM scheme. We will also investigate whether it plays a role in other popular schemes such as penalty methods. Another research direction that we plan to pursue is improved numerical stabilization of ROMs whose velocity-pressure ROM spaces do not satisfy the inf-sup/LBB condition. Finally, we plan to study the impact of different projection schemes [9] on AC, projection, and penalty methods in a ROM setting.

Acknowledgments. We thank the three reviewers for their comments and suggestions that have improved the manuscript.

REFERENCES

- A. ABDULLE AND O. BUDÁČ, A Petrov-Galerkin reduced basis approximation of the Stokes equation in parameterized geometries, C. R. Math. Acad. Sci. Paris, 353 (2015), pp. 641–645.
- [2] I. AKHTAR, A. H. NAYFEH, AND C. J. RIBBENS, On the stability and extension of reducedorder Galerkin models in incompressible flows, Theoret. Comput. Fluid Dyn., 23 (2009), pp. 213–237.
- [3] O. AXELSSON AND I. GUSTAFSSON, Preconditioning and two-level multigrid methods of arbitrary degree of approximation, Math. Comp., 40 (1983), pp. 219–219, https://doi.org/10.1090/ S0025-5718-1983-0679442-3.
- [4] M. AZAÏEZ, T. CHACÓN REBOLLO, AND S. RUBINO, Streamline Derivative Projection-Based POD-ROM for Convection-Dominated Flows. Part I: Numerical Analysis, arXiv e-prints, 2017, arXiv:1711.09780.
- [5] F. Ballarin, A. Manzoni, A. Quarteroni, and G. Rozza, Supremizer stabilization of POD-Galerkin approximation of parametrized steady incompressible Navier-Stokes equations, Internat. J. Numer. Methods Engng., 102 (2015), pp. 1136-1161.
- [6] M. BERGMANN, C. H. BRUNEAU, AND A. IOLLO, Enablers for robust POD models, J. Comput. Phys., 228 (2009), pp. 516–538.
- [7] A. CAIAZZO, T. ILIESCU, V. JOHN, AND S. SCHYSCHLOWA, A numerical investigation of velocitypressure reduced order models for incompressible flows, J. Comput. Phys., 259 (2014), pp. 598–616.
- [8] M. A. CASE, V. J. ERVIN, A. LINKE, AND L. G. REBHOLZ, A connection between Scott-Vogelius and grad-div stabilized Taylor-Hood FE approximations of the Navier-Stokes equations, SIAM J. Numer. Anal., 49 (2011), pp. 1461-1481, https://doi.org/10.1137/100794250.
- [9] J. DE FRUTOS, B. GARCÍA-ARCHILLA, AND J. NOVO, Error analysis of projection methods for non inf-sup stable mixed finite elements: The Navier-Stokes equations, J. Sci. Comput., 74 (2018), pp. 426-455, https://doi.org/10.1007/s10915-017-0446-3.

- [10] V. DECARIA, W. LAYTON, AND M. MCLAUGHLIN, A conservative, second order, unconditionally stable artificial compression method, Comput. Methods Appl. Mech. Engrg., 325 (2017), pp. 733–747.
- [11] V. EIJKHOUT AND P. VASSILEVSKI, The role of the strengthened Cauchy-Buniakowskii-Schwarz inequality in multilevel methods, SIAM Rev., 33 (1991), pp. 405-419, https://doi.org/10. 1137/1033098.
- [12] L. Fick, Y. Maday, A. T. Patera, and T. Taddei, A stabilized POD model for turbulent flows over a range of Reynolds numbers: Optimal parameter sampling and constrained projection, J. Comput. Phys., 371 (2018), pp. 214–243.
- [13] J. A. FIORDILINO AND M. MCLAUGHLIN, An Artificial Compressibility Ensemble Timestepping Algorithm for Flow Problems, preprint, http://arXiv:1712.06271, 2017.
- [14] K. FRIEDRICHS, On certain inequalities and characteristic value problems for analytic functions and for functions of two variables, Trans. Amer. Math. Soc., 41 (1937), pp. 321–364, https://doi.org/10.2307/1989786.
- [15] J. L. Guermond, Un résultat de convergence d'ordre deux en temps pour l'approximation des équations de Navier-Stokes par une technique de projection incrémentale, ESAIM Math. Model. Numer. Anal. Numérique, 33 (1999), pp. 169–189, http://www.numdam.org/item/ M2AN_1999_33_1_169_0.
- [16] J. L. GUERMOND, P. MINEV, AND J. SHEN, An overview of projection methods for incompressible flows, Comput. Methods Appl. Mech. Engrg., 195 (2006), pp. 6011–6045, https://doi.org/10.1016/j.cma.2005.10.010.
- [17] M. GUNZBURGER, N. JIANG, AND M. SCHNEIER, An ensemble-proper orthogonal decomposition method for the nonstationary Navier-Stokes equations, SIAM J. Numer. Anal., 55 (2017), pp. 286-304, https://doi.org/10.1137/16M1056444.
- [18] B. HAASDONK AND M. OHLBERGER, Reduced basis method for finite volume approximations of parametrized linear evolution equations, ESAIM Math. Model. Numer. Anal., 42 (2008), pp. 277–302.
- [19] J. S. HESTHAVEN, G. ROZZA, AND B. STAMM, Certified Reduced Basis Methods for Parametrized Partial Differential Equations, Springer, Cham, Switzerland, 2015.
- [20] J. G. HEYWOOD AND R. RANNACHER, Finite element approximation of the nonstationary Navier-Stokes problem. I. Regularity of solutions and second-order error estimates for spatial discretization, SIAM J. Numer. Anal., 19 (1982), pp. 275-311, https://doi.org/10. 1137/0719018.
- [21] M. HINZE AND S. VOLKWEIN, Proper orthogonal decomposition surrogate models for nonlinear dynamical systems: Error estimates and suboptimal control, in Dimension Reduction of Large-Scale Systems, P. Benner, D. C. Sorensen, and V. Mehrmann, eds., Springer, Cham, Switzerland, 2005, pp. 261–306.
- [22] P. HOLMES, J. L. LUMLEY, AND G. BERKOOZ, Turbulence, Coherent Structures, Dynamical Systems and Symmetry, Cambridge University Press, Cambridge, UK, 1998.
- [23] T. ILIESCU AND Z. WANG, Are the snapshot difference quotients needed in the proper orthogonal decomposition?, SIAM J. Sci. Comput., 36 (2014), pp. A1221–A1250.
- [24] T. ILIESCU AND Z. WANG, Variational multiscale proper orthogonal decomposition: Navier-Stokes equations, Numer. Methods Partial Differential Equations, 30 (2014), pp. 641–663.
- [25] N. JIANG AND W. LAYTON, An algorithm for fast calculation of flow ensembles, Int. J. Uncertain. Quantif., 4 (2014), pp. 273–301.
- [26] V. John, Finite Element Methods for Incompressible Flow Problems, Springer Ser. Comput. Math., Springer International Publishing, New York, NY, 2016.
- [27] C. JORDAN, Essai sur la geometrie a n dimensions, Amer. Math. Monthly, 3 (1875), pp. 103–174.
- [28] A. V. Knyazev and M. E. Argentati, Principal angles between subspaces in an A-based scalar product: Algorithms and perturbation estimates, SIAM J. Sci. Comput., 23 (2002), pp. 2008–2040, https://doi.org/10.1137/S1064827500377332.
- [29] K. Kunisch and S. Volkwein, Galerkin proper orthogonal decomposition methods for parabolic problems, Numer. Math., 90 (2001), pp. 117–148.
- [30] W. LAYTON, Introduction to the Numerical Analysis of Incompressible Viscous Flows, SIAM, Philadelphia, PA, 2008.
- [31] W. LAYTON, C. C. MANICA, M. NEDA, AND L. G. REBHOLZ, Numerical analysis and computational testing of a high accuracy Leray-deconvolution model of turbulence, Numer. Methods Partial Differential Equations, 24 (2008), pp. 555–582.
- [32] A. LOGG, K. MARDAL, AND G. WELLS, Automated Solution of Differential Equations by the Finite Element Method: The FEniCS Book, Springer Science & Business Media, New York, NY, 2012.

- [33] B. MOHAMMADI, Principal angles between subspaces and reduced order modelling accuracy in optimization, Struct. Multidiscip. Optim., 50 (2014), pp. 237–252, https://doi.org/10.1007/ s00158-013-1043-1.
- [34] M. MOHEBUJJAMAN, L. G. REBHOLZ, X. XIE, AND T. ILIESCU, Energy balance and mass conservation in reduced order models of fluid flows, J. Comput. Phys., 346 (2017), pp. 262–277.
- [35] B. R. NOACK, M. MORZYNSKI, AND G. TADMOR, Reduced-Order Modelling for Flow Control, Springer-Verlag, Cham, Switzerland, 2011.
- [36] B. R. NOACK, P. PAPAS, AND P. A. MONKEWITZ, The need for a pressure-term representation in empirical Galerkin models of incompressible shear flows, J. Fluid Mech., 523 (2005), pp. 339–365.
- [37] A. PROHL, Projection and Quasi-Compressibility Methods for Solving the Incompressible Navier-Stokes Equations, Springer, New York, NY, 1997, https://doi.org/10.1007/ 978-3-663-11171-9.
- [38] A. QUARTERONI, A. MANZONI, AND F. NEGRI, Reduced Basis Methods for Partial Differential Equations: An Introduction, Springer, New York, NY, 2015.
- [39] T. C. Rebollo, E. D. Ávila, M. G. Marmol, F. Ballarin, and G. Rozza, On a certified Smagorinsky reduced basis turbulence model, SIAM J. Numer. Anal., 55 (2017), pp. 3047–3067, https://doi.org/10.1137/17M1118233.
- [40] S. Rubino, Numerical Analysis of a Projection-Based Stabilized POD-ROM for Incompressible Flows, preprint, http://arxiv.org/abs/1907.09213, 2019.
- [41] J. R. SINGLER, New POD error expressions, error bounds, and asymptotic results for reduced order models of parabolic PDEs, SIAM J. Numer. Anal., 52 (2014), pp. 852–876.
- [42] L. Sirovich, Turbulence and the dynamics of coherent structures. Parts I-III, Quart. Appl. Math., 45 (1987), pp. 561–590.
- [43] G. Stabile and G. Rozza, Finite volume POD-Galerkin stabilised reduced order methods for the parametrised incompressible Navier-Stokes equations, Comput. & Fluids, 173 (2018), pp. 273–284.
- [44] K. VEROY AND A. T. PATERA, Certified real-time solution of the parametrized steady incompressible Navier-Stokes equations: rigorous reduced-basis a posteriori error bounds, Internat. J. Numer. Methods Fluids, 47 (2005), pp. 773-788.
- [45] S. Volkwein, Condition number of the stiffness matrix arising in POD Galerkin schemes for dynamical systems, PAMM. Proc. Appl. Math. Mech., 4 (2004), pp. 39–42, https: //doi.org/10.1002/pamm.200410010.
- [46] J. WELLER, E. LOMBARDI, M. BERGMANN, AND A. IOLLO, Numerical methods for low-order modeling of fluid flows based on POD, Internat. J. Numer. Methods Fluids, 63 (2010), pp. 249–268.
- [47] D. Wells, Z. Wang, X. Xie, and T. Iliescu, An evolve-then-filter regularized reduced order model for convection-dominated flows, Internat. J. Numer. Methods Fluids, 84 (2017), pp. 598—615.
- [48] L. WOF AND A. SHASHUA, Kernel principal angles for classification machines with applications to image sequence interpretation, in Proceedings of the 2003 IEEE Computer Society Conference on Computer Vision and Pattern Recognition, https://doi.org/10.1109/CVPR. 2003.1211413.
- [49] M. YANO, A space-time Petrov-Galerkin certified reduced basis method: Application to the Boussinesq equations, SIAM J. Sci. Comput., 36 (2014), pp. A232–A266.